Tellus (2007), 59B, 633–641
Printed in Singapore. All rights reserved

© 2007 The Authors
Journal compilation © 2007 Blackwell Munksgaard

TELLUS

A numerical study of influences of urban land-use change on ozone distribution over the Pearl River Delta region, China

By X.M. WANG[1]*, W.S. LIN[1], L.M. YANG[2], R.R. DENG[3] and H. LIN[2], [1]*School of Environmental Science and Engineering, Sun Yat-sen University, Guangzhou 510275, China;* [2]*Joint Laboratory for Geo-Information Science, Institute of Space and Earth Information Science, the Chinese University of Hong Kong, Hong Kong;* [3]*School of Geographical Science and Planning, Sun Yat-sen University, Guangzhou, China*

(Manuscript received 30 April 2006; in final form 26 January 2007)

ABSTRACT

Atmospheric dynamical and chemical models are conducted to explore impacts of urban land-use change on ozone concentrations over the Pearl River Delta (PRD) region, China. Two scenarios of land-use distributions are used to represent early 1990s and current urban land-use distributions. Urbanization increases 2-d averaged daytime (nighttime) temperature by 0.8 °C (1.5 °C) and reduces wind speed by about 20% over the PRD urban areas. The daytime boundary layer depth is up to 400 m deeper, while there is a 50-m increase during nighttime. The combination of these seemly subtle changes in meteorological conditions is able to prompt detectable changes in surface O_3 concentration (4–15 ppbv) over major PRD urban areas. Nighttime O_3 concentration enhancement is greater than daytime in the urban expansion regions (e.g. 10 ppbv daytime and 15 ppbv nighttime). Areas with main O_3 concentrations increase coincide with the areas of increased temperature and decreased wind speed, and the timing of maximum ozone concentration increase occurs a few hours later than maximum temperature increase and wind-speed reduction. Moreover, planetary boundary layer depth also plays an important role in modulating vertical transport of O_3, which can lead to daytime surface ozone concentrations reduction in some regions even with increasing temperatures.

1. Introduction

The Pearl River Delta (PRD) region, an area of about 41 700 km^2 located in the southern part of Guangdong Province in China, has experienced remarkable economic development and urbanization in the past two decades. Urban area counts for 60% in the total land use, which is two times higher than the Chinese national averaged level. The fast urbanization can significantly modify local and regional meteorological conditions. For instance, under clear skies and light wind conditions, cities are warmer than surrounding rural environments, that is, urban heat islands (UHIs) of up to 10 °C can form due to urban-rural differences (Bornstein, 1987). These urban-rural differences profoundly modify the surface energy budgets which can change the mixing layer depth and thermal structures in the boundary layer. Furthermore, urban areas are able to alter wind velocities (Bornstein and Johnson, 1977) and precipitation patterns (Changnon and Huff, 1986). Climatologic data indicate that, compared to the long-term average, the mean winter temperature of southern China increased by approximately 0.326° per decade for the past 37 yr (Liang and Wu, 1999). These modifications in meteorological conditions can significantly alter the chemistry of the lower troposphere and change the formation of secondary pollutants in the atmosphere (Wang et al., 2005a). In recent years severe air-pollution episodes with high ozone (O_3) and poor visibility occur in an alarming frequency throughout PRD (Lee and Sequeira, 2001; Wang et al., 2001). Ambient NO_x concentrations in the PRD have been the highest in China since 1985. Currently O_3 and particle matter are the most concerned air pollutants in the PRD (http://www.gdepb.gov).

Previous studies on regional land-use change within the PRD area were generally conducted at a local scale (one city or a few counties or a single Landsat scene) (Seto et al. 2002; Weng, 2002). Recently, Lo et al. (2006, 2007), using an atmospheric model and a three-dimensional particle trajectory model, pointed out that urbanization in the PRD can modify regional land–sea-breeze circulations and potentially enhance the pollutant trapping, and therefore may contribute to the overall poor air quality in the region. Nevertheless, impacts of urbanization on air quality in the PRD have not been quantified. Recent development in

*Corresponding author.
e-mail: eeswxm@mail.sysu.edu.cn
DOI: 10.1111/j.1600-0889.2007.00271.x

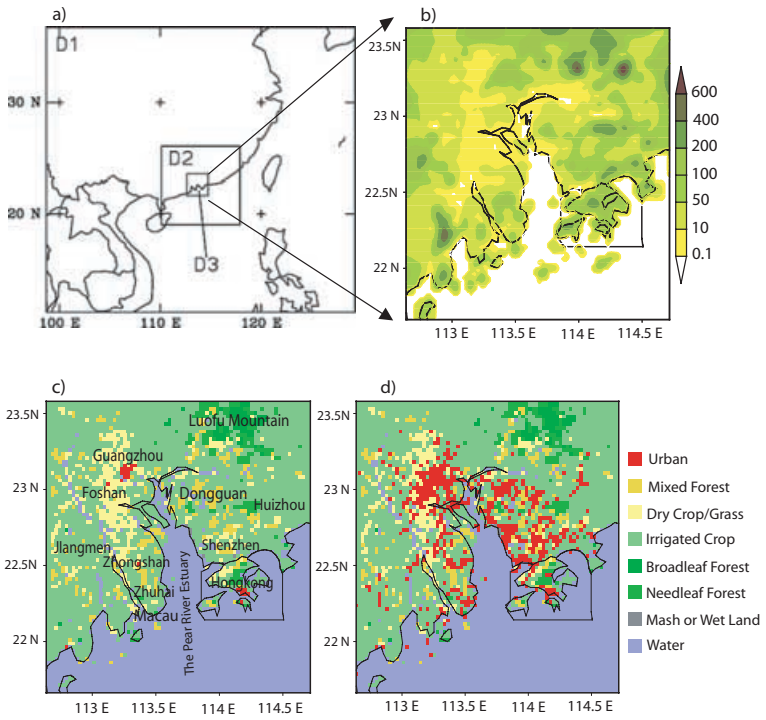

Fig. 1. MM5 modelling domains and land-use data sets used for MM5 simulations: (a) MM5 nested domains. Domain 1 (D1): 27-km grid spacing; Domain 2 (D2): 9-km grid spacing; Domain 3 (D3): 3-km grid spacing, (b) terrain height in D3, (c) 1992–1993 USGS data used in MM5 V3.7 for D3 and (d) Land-use data based on 2004 0.5-km MODIS products aggregated to 3-km for D3. The only change between (c) and (d) is the urban areas marked in red colour.

high-resolution land cover data, advanced land surface model, and improved planetary boundary layer (PBL) parametrization schemes allow more realistic simulations of the PBL structures in mesoscale numerical models (Chen and Dudhia, 2001). Therefore, in this work, we combine mesoscale atmospheric and chemical models to investigate how ozone distributions respond to changes in atmospheric conditions due to urbanization in the PRD because ozone is the most important oxidant and indicator of photochemical smog. Here, we primarily focus on the analysis of ozone modifications to meteorological conditions change and do not consider chemical processes and emissions changes response on ozone concentration. A high-pollution episode of 29–30 October 2004, where the API (Air Pollution Index) as high as 100 in Guangzhou, is selected for this case study.

The reminder of the paper is organized as follows. In Section 2, we describe the numerical modelling systems used in this study. A brief discussion of the design of numerical experiments discussed in this paper is also provided. Section 3 presents discussions about impacts of urbanization on meteorological conditions and on surface ozone concentration. A summary and concluding remarks are presented in Section 4.

2. Description of models and numerical experiments

2.1. The MM5 model

The coupled fifth-generation Pennsylvania State University—National Center for Atmospheric Research non-hydrostatic Mesoscale Model (MM5)—land surface modelling system is used in this study. MM5 (Grell et al. 1994) is configured for the current study with three two-way interactive grids having horizontal grid spacings of 27, 9 and 3 km and grid point dimensions of 127 × 118, 97 × 97 and 79 × 79, respectively. The locations of the nested domains are shown in Fig. 1a. The coarse outer domain, D1, comprises a large portion of China and extends farther south into the Southern China sea, and the second domain D2 covers most of Guangdong province. To better capture influences of UHIs and urbanization on the PRD, a 3-km grid, in conjunction with high-resolution land-use maps, is used for the MM5 inner domain. As shown in Fig. 1b there is a gentle increase in terrain height (∼400 meters) from cities to their surrounding rural areas in the PRD. MM5 is a terrain-following model that uses the sigma vertical coordinate. The same 22 sigma levels were specified for all simulations. Pressure at the top of the model, where a radiative boundary condition is used, is 100 hPa. The lowest half-sigma level is located at 38 m above ground level. Since a major objective of the current study is to examine the effect of urbanization on PBL structures, vertical resolution is significantly enhanced in the lowest 1-km atmosphere.

Table 1 shows the parametrization schemes in MM5 and input/output data. Medium range forecast (MRF) PBL scheme (Hong and Pan, 1996) and the NCAR Community Climate Model (CCM2) longwave and shortwave scheme (Hack et al, 1993) were used in all domains. An explicit microphysical scheme that predicts rain, snow, graupel, cloud water and cloud ice is used on all domains. This scheme is based on Reisner et al. (1998) but has been modified to include graupel and ice number

Table 1. Input/output for MM5 and STEM-2K1 models

Models	Input	Output	Parametrizations
MM5	$1^\circ \times 1^\circ$ resolution NCEP global reanalysis data	Meteorological fields on 27-, 9- and 3-km grids that include: 3-D: wind, temperature, pressure, rain water mixing ratio, cloud water ratio, water vapour ratio 2-D: ground temperature, boundary layer height, precipitation rate, u^*, w^*, p^*	PBL scheme: MRF Cumulus: Kain–Fritsch Microphysics: Reinser2 Radiation: Same as in CCM2 Noah LSM
STEM-2K1	Hourly output from MM5 meteorological fields on 27-, 9-, and 3-km grids Hourly emissions, chemical species initial and boundary conditions	3-D gas-phase species including SO_2, NO, NO_2, O_3, ethane, propane, formaldehyde, PAN etc., Photolysis rate, 3-D Aerosol including: BC, OC, PM2.5, PM10 etc.	SAPRC99 gas-phase chemical mechanism; online TUV for photolysis rates

concentration prediction equations. The Kain–Fritsch cumulus parametrization scheme (Kain and Fritsch, 1993) was used for the two outermost domains (D1 and D2), whereas no cumulus parametrization scheme was used for the finest domain (D3) because it was assumed that convection is reasonably well resolved by the explicit microphysics (Weisman et al, 1997).

The Noah land surface model (LSM) coupled to the MM5 (Chen and Dudhia, 2001; Ek et al., 2004; Chen 2005) is based on the Oregon State University (OSU) LSM (Pan and Mahrt 1987). The LSM has a single canopy layer and predicts volumetric soil moisture and temperature in four soil layers. The depths of the individual soil layers from top to bottom are 0.1, 0.3, 0.6 and 1.0 m. The root zone is contained in the upper 1 m (top three layers) no matter what land-use type. The Noah LSM urban enhancements by Liu et al. (2006) included: (1) increasing the roughness length to 0.8 m to better account for the drag due to buildings; (2) reducing the surface albedo to 0.15, where this reduction accounts for the shortwave radiation trapping in the urban canyons; (3) increasing the volumetric heat capacity to 3.0×10^6 J m^{-3} K^{-1} and the soil thermal conductivity to 3.24 W m^{-1} K^{-1} to be more consistent with the prevailing concrete or asphalt materials and (4) reducing the green vegetation fraction to reduce evaporation. The performance of the MM5 modelling system coupled to this simple urban treatment was verified with surface and wind profiler data for the Oklahoma City area (Liu et al., 2006) and for the PRD region (Lo et al., 2006a).

The initial and boundary conditions are interpolated from the 1-degree resolution NCEP global reanalysis data (Kistler et al., 2001) to the MM5 coarse domain (D1) with a grid spacing of 27 km and to the 22 sigma levels. Surface and upper-air conventional observational data are incorporated into the analysis using a Cressman-type analysis scheme. Initial conditions for the two finer domains are obtained by interpolating from the outer domain. Because the MM5 simulations are initialized with a cold start (no initial hydrometeors), it takes at least 12 hr on average for the model to spin up (Colle et al., 1999). In this study, the simulation started from 0000 UTC 28 October and ended at 2300 UTC 30 October 2004. The first 16-hr MM5 simulation is used to spin up the model.

2.2. *Land-use data sets and sensitivity experiments*

Two land-use scenarios are used for the PRD region in the MM5 D-3 in this case study to explore the effect of urban expansion. The United States Geological Survey (USGS) global land-use map in MM5 is based on 1992–1993 1-km Advanced Very High Resolution Radiometer (AVHRR) data (see Fig. 1c), which, to a large degree, reflects the distribution of cities (mainly Guangzhou and Hong Kong) in the late 1980s in PRD. By contrast, an updated land-use based on the 2004 500-m Moderate Resolution Imaging Spectroradiometer (MODIS) data is used to refer to today's distributions of cities in PRD (see Fig. 1d) with rapidly urbanized areas centred in Guangzhou, Foshan, Dongguan and Shenzhen. The MODIS instrument provides high radiometric sensitivity (12 bit) in 36 spectral bands in wavelength ranging from 0.4 μm to 14.4 μm. The images used to identify urban areas are composed of the first three channels of MODIS with the resolution of 500 m. The colour of urbanized areas in these images is dark grey, outstanding from other land cover, and can easily be identified. The 500-m MODIS data are aggregated onto 3-km D3 using the same approach in MM5 to aggregate the 1-km USGS land-use data.

With the MM5/Noah coupled model, two simulations are conducted using the same initial and lateral boundary conditions, the same physics packages, and the same model configurations. The only difference between these two simulations is the land-use map: the control simulation (PRE-URBAN) uses the USGS AVHRR land-use map mimicking the PRD land-use distribution prior to the rapid urban and industrial development occurred in the last two decades; the sensitivity simulation

(URBAN) uses the MODIS land-use data describing today's land-use distribution.

2.3. The stem-2K1 model

In this study, STEM (Sulfur Transport and dEposition Model)-2K1 (Carmichael et al., 2003a,b; Tang et al., 2003) is executed, on the same grids as MM5 (i.e. 27-, 9- and 3-km grid) using the PRE-URBAN and URBAN land use maps to investigate the influence of land use change on ozone over the PRD. This model was used in the TRACE-P (Transport and Chemical Evolution over the Pacific) experiment and compared with observed data in the PRD region by Wang et al. (2005b). STEM-2K1 is driven by MM5 meteorological output in the three domains, which has the same vertical and horizontal resolution with MM5. Table 1 shows the connection between STEM-2K1 and MM5. Time interpolation was performed to treat the rapid changes in PBL, especially in the morning and evening. For chemical species initial and boundary conditions, those profiles obtained from the TRACE-P aircraft observations were used for the coarse domain. The initial and boundary conditions for the inner two domains were interpolated from corresponding mother domain. Emissions were interpolated into each domain from 6 min resolution emission inventory.

The key module in STEM-2K1 is the SAPRC99 gas-phase chemical mechanism (Tang et al., 2003) and the second- order implicit Rosenbrock method (Verwer et al., 1997) for the chemical integrator is employed in these simulations. SAPRC99 contains 93 species and 213 chemical reactions, including 30 photolysis reactions.

Clouds and aerosols have important impacts on photolysis rates, hence influence photochemistry. The online TUV (Tropospheric Ultraviolet-Visible) model (Madronich and Flocke, 1999) was used to consider the influences of clouds, aerosols, and gas-phase absorptions due to O_3, SO_2, and NO_2 on photolysis rates. TUV employs MM5 outputted cloud water content to derive cloud optical properties. The optical properties of water clouds were calculated with a simple scheme (Madronich, 1987). We adopted the method of Ebert and Curry (1992) to estimate ice cloud optical properties. At each integrating time step, the online TUV inputs aerosol concentrations from the STEM main module and converts them from mass concentrations to aerosol optical properties according to Hess et al. (1998). Here we assume all aerosols are mixed externally. TUV outputs photolysis rates for SAPRC99 mechanism. Here the TUV has a higher top (80km) than that of the chemical-transport domain ($\sim$15 km). The interaction of TUV with STEM was described by Tang et al. (2003). The upper layers were used to compute the ozone absorption. The input data is daily variations in ozone columns that are accounted for by using the observed TOMS (Total Ozone Mapping Spectrometer) total columns. Zonal mean values are used for the regions that the TOMS satellite did not cover. Ozone profiles calculated by STEM are used in TUV for the tropospheric component, and the upper atmosphere ozone absorption column is calculated by the difference between TOMS ozone and STEM column ozone.

The anthropogenic emission rates used in this analysis are based on the estimates of Streets et al. (2003). Estimates of emission from individual sectors (i.e. industry, power, domestic, transportation and shipping) are included in the analysis. Measurements obtained in the TRACE-P experiment during February and April, 2001 are used in conjunction with regional modelling analysis to evaluate emission estimates for Asia (Carmichael et al., 2003a, b). It was found that the emission inventories are of sufficient quality to support preliminary studies of ozone production. Biomass burning emission (from open burning) for Southeast Asia are based on the March averaged estimates for the year of 2001(Woo et al., 2003). Biogenic emissions came from GEIA (Guenther et al., 1995). The emissions are gridded using the methodology described in Woo et al. (2003). Lighting NO_x emissions were diagnosed from the meteorological model according to deep convective intensities (Pickering et al., 1998). Emissions of dust, generated from the arid and semi-arid regions in Asia, were calculated online using model calculated friction velocities according to the method of Nickling and Gillies (1993) and Liu and Westphal (2001). Sea salt emissions were also calculated online following Monahan et al. (1986). The simulation length is the same as MM5. As our main objective is to explore the influences of urban-induced changes in meteorological conditions on air quality, we use the same surface biogenic and industrial emission rates (reflecting today's situation) in both land use maps. The impacts of emission rate changes will be investigated in the future.

3. Results and analysis

3.1. Influences of urban expansion on meteorological conditions

In the study of Lin et al. (2007), a total of 31 MM5 simulations (every day) in relation to the South China on October 2004, were conducted. Comparing with observed monthly mean temperature, the simulated monthly mean 2-m temperature is close to the observations in the northern part of Guangdong province but has lower bias ($\sim$1.2 $^{\circ}$C) near the coastal urban zones. Fig. 2 shows averaged differences of daytime and nighttime wind speed, temperature and PBL depth at 38 m above ground level between URBAN and PRE-URBAN MM5 simulations for D3. The simple urban land-use treatment in MM5/Noah has demonstrated its ability to capture main features of UHI (Liu et al., 2006; Lo et al., 2006a). After previous dry cropland was changed to current urban land, UHI effect becomes evident. MM5 simulations show obviously nighttime temperature enhancement in all urban expansion districts, which is typical UHI effect. It should be noted that Guangzhou is an urban site in both PRE-URBAN and URBAN scenarios. However, URBAN scenario has much

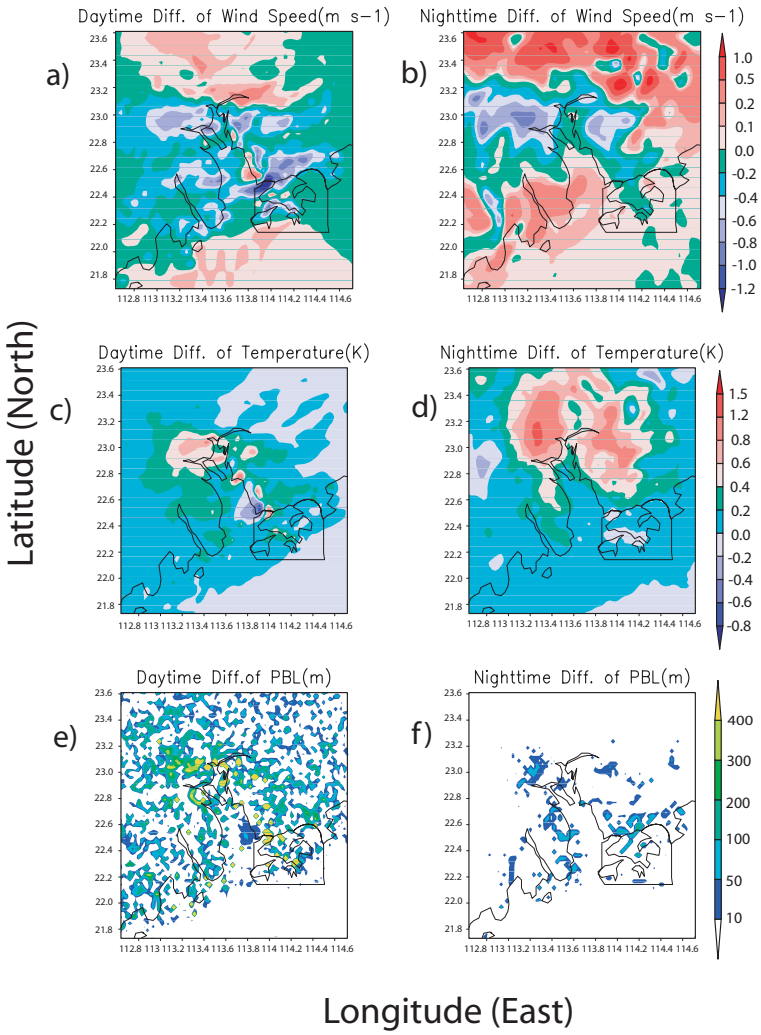

Fig. 2. Differences of weather variables at 38 m above the ground between URBAN and PRE-URBAN simulations (URBAN minus PRE-URBAN) averaged for the daytime and nighttime simulation period. (a) Daytime wind speed (m s^{-1}), (b) nighttime wind speed (m s^{-1}), (c) daytime temperature (K), (d) nighttime temperature (K), (e) daytime PBL depth (m) and (f) nighttime PBL depth (m).

broader urban areas than PRE-URBAN scenario in Guangzhou surrounding areas. MM5 simulations show the highest temperature enhancement in Guangzhou (Figs. 2c and d) and the second temperature enhancements are in Dongguan and Shenzhen. The increase in temperature in the Guangzhou district is up to 0.8 °C in the daytime and 1.5 °C at the nighttime due to strong turbulent mixing after urbanization in the daytime.

Areas with main reduction in wind speed also coincide with the fastest urban expansion regions such as Guangzhou, Dongguan and Shenzhen due to increase surface roughness length. Wind speed in those regions decrease up to 1.0 m s^{-1}, about 20% change. This change also show a diurnal feature: the strongest wind velocity decrease appeared at night due to increased surface roughness length in URBAN scenario and relatively weak vertical exchange of wind momentum at night. The maximum reduction in wind speed due to urbanization occurs at night, which is well correlated with large increase in temperature.

The spatial distributions of the daytime and nighttime mean differences of the PBL depth between URBAN and PRE-URBAN are shown in Figs. 2e and f respectively. The PBL development over urban areas is significantly enhanced by urban expansion, as the PBL depth is up to 400 m deeper during the daytime in Guangzhou area, while there is a 50-m increase of the PBL depth during the nighttime.

3.2. *Influences of urbanization on O_3 concentration*

We have seen so far that urbanization can modify temperature, wind speed, and the PBL mixing-layer depth and stability. In this section, we focus on impacts of those modified meteorological conditions on spatial and temporal distributions of ozone (O_3) concentration, because it is the traditional indicator of photochemical smog in the PRD. Figure 3 shows influences of urban expansion on daytime and nighttime averaged surface O_3 concentrations. While surface O_3 concentrations over major cities increase both during daytime and during nighttime, the nighttime enhancements in O_3 concentrations outpace those during daytime in the urban expansion regions. For instance, during

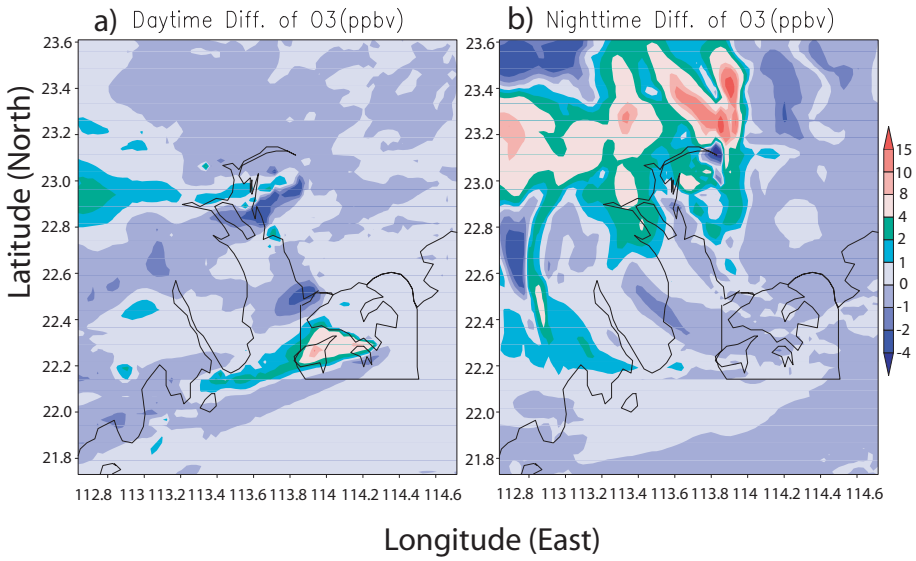

Fig. 3. Differences of surface ozone concentration (ppbv) between URBAN and PRE-URBAN simulations (URBAN minus PRE-URBAN). (a) Averaged for the daytime and (b) averaged for nighttime simulation.

daytime, the maximum O_3 concentrations augmentation occurs over the Hongkong area (∼10 ppbv) with a second maximum over the Guangzhou area (∼4 ppbv). The nighttime maximum O_3 increase has larger amount (>15 ppbv) and is located over major urban expansion areas such as Guangzhou and Dongguan. Areas with main O_3 concentrations increase generally coincide with the areas of temperature increase and wind-speed reduction. These results are consistent with previous studies showing the direct link between increased ozone concentrations and higher temperatures (Sillman and Samson, 1995; Aw and Kleeman, 2001). Nevertheless, it should be noted that, in the daytime, some urban regions such as Foshan and suburb of Guanghou experience slight reduction in surface ozone concentration even with higher temperature and lighter wind in those areas. This implies that the temperature enhancement alone is not sufficient to explain changes in surface O_3 concentrations. Because in the real world, temperature change will likely be coupled to changes in other meteorological variables such as the PBL depth that will in turn affect O_3 concentrations. In fact, deeper daytime, convective boundary layer over major urbanized areas can lead to stronger vertical mixing that dilutes surface O_3 concentrations. For example, over the Guangzhou district (Fig. 2), the daytime increase in the PBL depth (>400 m) is greater than the nighttime increase (∼100 m). Hence, the surface O_3 is transported to upper mixing layer and the O_3 concentration increases throughout the entire mixing layer up to 1700 m (not shown). By contrast, despite the slightly unstable, nocturnal surface layer caused by more pronounced nighttime UHI, the increase of O_3 is mainly confined within the lowest 150 m above the ground, leading to higher surface O_3 concentration. Therefore, the more enhanced nighttime surface O_3 is a consequence of slightly higher surface temperature (Figs. 2c and d) and, more importantly, of shallower mixing layer (Figs. 2e and f). The other reason for large nocturnal increase in surface O_3 concentration is weaker wind speed, which reduces horizontal transport of pollutants and results in local O_3 accumulation.

In order to further investigate the relationship between temperature and wind-speed perturbation and surface O_3 concentrations changes, we examined the diurnal cycle of the difference of O_3 concentrations between URBAN and PRE-URBAN simulations as function of surface temperature and wind speed in the Guangzhou district (Fig. 4). Clearly, surface O_3 concentrations change has stronger relationship with temperature variations than with surface wind speed. Note that the maximum O_3 concentrations increase happens around 0004 LST, while the maximum temperature increase happens at midnight and the maximum wind-speed reduction happens at 2200 LST. The temperature increase happens during mid-night with O_3 concentrations increase. However, surface ozone increases from 0200 LST to dawn (particularly for the second night) with decreasing temperature because of more ozone are confined in the surface layer.

4. Summary and conclusions

The PRD region has experienced remarkably fast economic development and rapid urbanization in the past two decades, forming a virtual PRD city cluster with a population of 50 million. Accompanying to such industrial and urban expansion, the air quality in PRD has been increasingly deteriorated in recent years. In this work, mesoscale atmospheric MM5 and chemistry STEM-2K1 models are employed to investigate the degree to which extensive urbanization can influence ozone concentrations over the PRD, which is a major indicator of photochemical

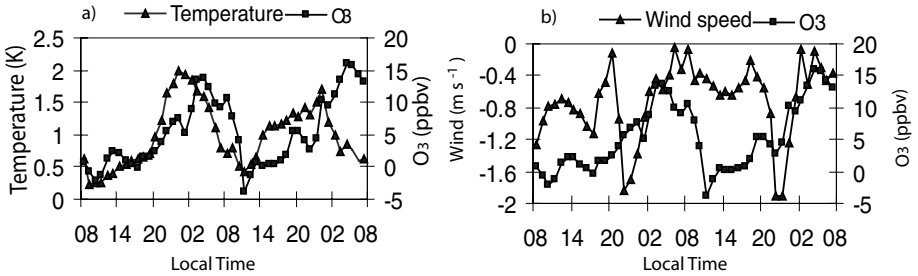

Fig. 4. Diurnal cycle of the difference between URBAN and PRE-URBAN at an urban site over the Guangzhou district. (a) Temperature and O_3 and (b) wind speed and O_3.

smog. For a high-pollution case study (29–30 October 2004), two types of urban land-use database, representing late 1980′s and current urban land cover in PRD, are used in MM5 simulations. Meteorological conditions generated in these two MM5 simulations are then used to drive the chemistry STEM-2K1 model to simulate temporal and spatial distribution of ozone under these two meteorological scenarios.

MM5 simulations show that areas with significant changes in meteorological conditions coincide with the fastest urban expansion regions such as Guangzhou, Dongguan, and Shenzhen. Maximum changes in temperature and wind speed usually occur between late evening and midnight, as expected from the UHI effect. Two-day averaged temperature increase up to 0.8 °C in the daytime and 1.5 °C at the nighttime over urban regions, while wind speed reduces up to 1.0 m s^{-1} in the lower atmosphere. The maximum reduction in wind speed due to urbanization occurs at night, which is well correlated with large increase in temperature. The PBL depth is up to 400 m deeper in the daytime, while there is 50 m increase at the nighttime.

When combined, those seemly small changes in meteorological conditions are able to prompt detectable changes in ozone concentration. Generally, averaged ozone concentrations increase coincides with temperature increase and wind-speed reduction in urban areas. For instance, 2-d averaged daytime O_3 concentration increases up to 10 ppbv over the Hong Kong metropolitan areas in the downwind direction of the Guangzhou urban area (Fig. 3a), while about 4 ppbv increase in O_3 concentrations is observed in Guangzhou areas. However, the PBL depth also plays an important role in the daytime vertical transport, which can lead to surface ozone concentrations reduction in some regions, even with increased temperatures in those areas. This is because on one hand, stronger daytime urban heating certainly helps increase ozone concentration. On the other hand, however, it often results in a deeper mixing layer with more vigorous transport of surface ozone to upper boundary layer and hence dilute surface ozone concentration. During nighttime, the increase in O_3 concentration, resulted from nocturnal urban heat island effects and more wind-speed reduction, is more confined to near surface layer because of generally stable boundary layer. Surface O_3 concentrations change has stronger relationship with temperature variations than with wind speed, but the timing of maximum ozone concentrations increase occurs a few hours later compared to maximum temperature increase and wind-speed reduction.

This study provides a first step to understanding the impacts of rapid urbanization on regional and local ozone distributions in the PRD region, and these results can be valuable for state and local policy makers for future development planning. Nevertheless, more comprehensive studies need to be conducted in the future to invoke different surface emissions scenarios and to investigate urban effects under different weather regimes.

5. Acknowledgments

The authors wish to thank two anonymous reviewers for their valuable comments and suggestions, which substantially improved this manuscript. The work described in this paper was supported by a grant from the 973 project (2007CB407303) China and partially supported by NSFC (40645024). This research was partially supported by a grant from the Research Grants Council of the Hong Kong Special Administrative Region (No. CUHK4642/05H). This research was also partially supported by State Key Laboratory of Atmospheric Boundary Layer Physics and Atmospheric Chemistry (LAPC) of Institute of Atmospheric Physics (IAP), China(LAPC-KF-2006–12).

References

Aw, J. and Kleeman, M. 2003. Evaluating the first-order effect of intraannual temperature variability on urban air pollution. *J. Geophys. Res.* **108**(D12), 4365, doi:10.1029/2002JD002688.

Bornstein, R. D. and Johnson, D. S. 1977. Urban-rural wind velocity differences. *Atmos. Environ.* **11**, 597–604.

Bornstein, R. 1987. Urban climate models: nature, limitations, and applications. *Meteorol. and Atmos. Physics* **38**, 185–194.

Carmichael, G. R., Tang, Y., Kurata, G., Uno, I., Streets, D. G. and co-authors. 2003a. Evaluating regional emission estimates using the TRACE-P observations. *J. Geophys. Res.* **108** (D21),8810, doi: 10.1029/2002JD003116.

Carmichael, G. R., Tang, Y., Kurata, G., Uno, I., Huang, H. and co-authors. 2003b. Regional-Scale chemical transport modeling in support of intensive field experiments: overview and analysis of the TRACE-P Observations. *J. Geophys. Res.* **108**(D21), 8823, doi: 10.1029/2002JD003117.

Changnon, S. A. and Huff, F. A. 1986. The urban-related nocturnal rainfall anomaly at St., Louis. *J. Clim. Appl. Meteor.* **25**, 1985–1995.

Chen, F. and Dudhia, J. 2001. Coupling an advanced land-surface/hydrology model with the Penn State/NCAR MM5 modeling system. Part I: Model implementation and sensitivity. *Mon. Wea. Rev.* **129**, 569–585.

Chen, F. 2005. Variability in global land surface energy budgets during 1987–1988 simulated by an offline land surface model. *Climate Dynamics*. doi: 10.1007/s00382–004–0439–4.

Colle, B. A., Westrick, K. J and Mass, C. F. 1999. Evaluation of MM5 and Eta-10 recipitation forecasts over the Pacific Northwest during the cool season. *Weather Forecast.* **14**, 137–156.

Ebert, E. E. and Curry, J. A. 1992. A parameterization of ice-cloud optical-properties for climate models. *J. Geophys. Res.* **97**, 3831–3836.

Ek, M. B., Mitchell, K. E., Lin, Y., Rogers, E., Grunmann, P. and co-authors. 2003. Implementation of Noah land-surface model advances in the NCEP operational mesoscale Eta mode. *J. Geophys. Res.* **108** (D22), No. 8851 NOV 29.

Grell, G. A., Dudhia, J. and Stauffer, D. R. 1994. A description of the fifth-generation Penn State/NCAR mesoscale model (MM5). NCAR Technical Note, NCAR/TN-398+STR, National Center for Atmospheric Research, Boulder, Colorado., 117.

Guenther, A., Hewitt, C. N., Erickson, D., Fall, R., Geron, C. and co-authors. 1995. A global-model of natural volatile organic-compound emissions. *J. Geophys. Res.* **100** (D5), 8873–8892.

Hack, J. J., Boville, B. A., Briegleb, B. P., Kiehl, J. T., Rasch, P. J. and co-authors. 1993. Description of the NCAR Community Climate Model (CCM2). NCAR Technical Note, NCAR/TN-382+STR, National Center for Atmospheric Research, Boulder, Colorado 108.

Hess, M., Koepke, P. and Schult, I. 1998. Optical properties of aerosols and clouds: the software package OPAC. *Bull. Am. Meteorol. Soc.* **79**(5), 831–844.

Hong, S. Y. and Pan, H. L. 1996. Nonlocal boundary layer vertical diffusion in a medium-range forecast model. *Mon. Wea. Rev.* **124**, 2322–2339.

Kain, J. S. and Fritsch, J. M. 1993. Convective parameterization for mesoscale models: the Kain–Fritsch scheme. The representation of cumulus convection in numerical models. *Meteor. Monogr.* **46**, 165–170.

Kistler, R., Kalnay, E., Collins, W., Saha, S., White, G. and co-authors. 2001. The NCEP-NCAR 50-year reanalysis: monthly means CD-ROM and documentation. *Bull. Amer. Meteor. Soc*. **82**, 247–268.

Lee, Y. L. and Sequeira, R. 2001. Visibility degradation across Hongkong: its components and their relative contributions. *Atmos. Environ.* **34**, 5861–5872.

Liang, J. Y. and Wu, S. S. 1999. Climatological diagnosis of winter temperature ariations in Guangdong. *J. Tropical Meteor.* **15**(3),221–229 (in Chinese).

Liu, M. and Westphal, D. L. 2001. A study of the sensitivity of simulated mineral dust production to model resolution. *J. Geophys. Res.* **106**, 18, 099–18, 112.

Lin, W. S., Sui, C. H., Yang, L. M., Wang, X. M., Dang, R. R. and co-authors. 2006. A numerical study of the influence of urban expansion on monthly climate in dry autum over Pearl River Dealta,China. *Theor. Appl. Climatol.* In press.

Liu, Y., Chen, F., Warner, T. and Basara, J. 2006. Verification of a Mesoscale Data-Assimilation and Forecasting System for the Oklahoma City Area During the Joint Urban 2003 Field Project. *J. Appl. Meteorol. Clim*. **45**, 912–929.

Lo, J., Lau, A., Chen, F. and Fung, J. 2007. Urban modification in a mesoscale model and the effects on the local circulation in the Pearl River Delta Region. *J. Appli. Meteorol.* in press.

Lo, J., Lau, A., Fung, J. and Chen, F. 2006b. Role of land-sea-breeze circulations modified by urbanization on air pollution in the Pearl River Delta region. *J Geophys. Res.* **111**, (D14104), doi:10.1029/2005JD006837.

Madronich, S. 1987. Photodissociation in the atmosphere: 1. Actinic flux and the effects of ground reflections and clouds. *J. Geophys. Res.,* **92**, 9740–9752.

Madronich, S. and Flocke, S. 1999. The role of solar radiation in atmospheric chemistry, in handbook of environmental chemistry. (ed. P. Boule). Springer-Verlag, Heidelberg1–26.

Monahan, E. C., Spiel, D. E. and Davidson, K. L. 1986. A model of marine aerosol generation via whitecaps and wave disruption, in oceanic Whitecaps, edited by E. C. Monahan and G. MacNiocaill, 167–174, D. Reidel, Norwell, Massachusetts.

Nickling, W. G. and Gillies, J. A. 1993. Dust emission and transport in Mali, West Africa. *Sedimentology* **40**, 859–868.

Pan, H. L. and Mahrt, L.1987. Interaction between soil hydrology and boundary-layer development. *Bound. Layer Meteor.* **38**, 185–202.

Pickering, K. E., Wang, Y. S., Tao, W. K., Price, C. and Muller, J. F. 1998. Vertical distributions of lightning NOx for use in regional and global chemical transport models. *J. Geophys. Res.* **103**, 31, 203–31, 231, 216.

Seto, K. C., Lu, J., Kaufmann, R. K., Woodcock, C. E., Song, C. and Huang, X. 2002. Monitoring land-use change in the Pearl River Delta using Landsat TM. *Int. J. Remote Sens.* **23**, 1985–2004.

Sillman, S. and Samson, P. J. 1995. Impact of temperature on oxidant photochemistry in urban, polluted rural and remote environments. *J.Geophys. Res.* **100**, 11 497–11 508.

Streets, D. G., Bond, T. C., Carmichael, G. R., Fernandes, S. D., Fu, Q. and co-authors. 2003. A year-2000 inventory of gaseous and primary aerosol emissions in Asia to support TRACE-P modeling and analysis. *J. Geophys. Res.* **108**(D21), 8809, doi:10.1029/2002JD003093.

Tang, Y., Carmichael, G. R., Uno, I., Woo, J. H., Kurata, G. and co-authors. 2003. Impacts of aerosols and clouds on photolysis frequencies and photochemistry during TRACE-P, part II: three-dimensional study using a regional chemical transport model. *J. Geophys. Res.* **108**(D21), 8822, doi: 10.1029/2002JD003100.

Verwer, J. G., Spee, E. J., Blom, J. G. and Hundsdorfer, W. H. 1997. A second order Rosenbrock method applied to photochemical dispersion problems. *Modelling, Analysis and Simulation (MAS)*, MAS-R9717, August 31.

Wang, T., Wu, Y. Y., Cheung, T. F. and Lam, K. S. 2001. A study of surface ozone and the relation to complex wind flow in Hongkong. *Atmos. Environ.* **35**, 3203–3215.

Wang, X. M., Tang, Y. H. and Carmichael, G. R. 2005a. A modeling study on regional air pollutions transport patterns over the pearl river delta in the fall season. *Mod. Phys. Lett. B* **19** (28–29), 1735–1738.

Wang, X. M., Carmichael, G. R., Chen, D. L. and Tang, Y. H. 2005b. Impacts of different emission sources on air quality during March

2001 in the Pearl River Delta (PRD) region. *Atmos. Environ.* **39**(29), 5227–5241.

Weisman, M. L., Skamarock, W. C. and Klemp, J. B. 1997. The resolution dependence of explicitly modeled convection. *Mon. Wea. Rev*. **125**, 527–548.

Weng, Q. 2002. Land use change analysis in the Zhujiang Delta of China using satellite remote sensing, GIS and stochastic modeling. *J. Environ. Manag.* **64**, 273–284.

Woo, J. H., Streets, D. G., Carmichael, G. R., Tang, Y. and co-authors. 2003. Biomass and biofuel emissions and their impact on trace gas distributions in Asia during the TRACE-P experiment. *J. Geophys. Res.* **108**(D21), 8812, doi:10.1029/2002JD003200.